Cell. Mol. Life Sci. (2011) 68:1593–1610
DOI 10.1007/s00018-010-0535-z

Cellular and Molecular Life Sciences

RESEARCH ARTICLE

Molecular mechanisms of centrosome and cytoskeleton anchorage at the nuclear envelope

Maria Schneider · Wenshu Lu · Sascha Neumann · Andreas Brachner · Josef Gotzmann · Angelika A. Noegel · Iakowos Karakesisoglou

Received: 18 May 2010 / Revised: 13 September 2010 / Accepted: 14 September 2010 / Published online: 5 October 2010

Abstract Cell polarization is a fundamental process underpinning organismal development, and tissue homeostasis, which requires an orchestrated interplay of nuclear, cytoskeletal, and centrosomal structures. The underlying molecular mechanisms, however, still remain elusive. Here we report that kinesin-1/nesprin-2/SUN-domain macromolecular assemblies, spanning the entire nuclear envelope (NE), function in cell polarization by anchoring cytoskeletal structures to the nuclear lamina. Nesprin-2 forms complexes with the kinesin-1 motor protein apparatus by associating with and recruiting kinesin light chain1 (KLC1) to the outer nuclear membrane. Similar to nesprin-2, KLC1 requires lamin A/C for proper NE localization. The depletion of nesprin-2 or KLC1, or the uncoupling of nesprin-2/SUN-domain protein associations impairs cell polarization during wounding and dislodges the centrosome from the NE. In addition nesprin-2 loss has profound effects on KLC1 levels, the cytoskeleton, and Golgi apparatus organization. Collectively these data show that NE-associated proteins are pivotal determinants of cell architecture and polarization.

Keywords Cell polarity · Centrosome · Cytoskeleton · KASH-domain · Kinesin-1 · Lamin A/C · Laminopathies · Nesprin

Abbreviations

AD	Gal4-activating domain
BD	Gal4-DNA-binding domain
β-gal	β-Galactosidase
CT	C-terminus
DN	Dominant negative
ER	Endoplasmic reticulum
G	Giant
GST	Glutathione-S-transferase
GFP	Green fluorescent protein
IF	Intermediate filament
KHC	Kinesin heavy chain
KLC	Kinesin light chain
MT	Microtubule
NE	Nuclear envelope
N2-SR	Nesprin-2 SR
NT	N-terminus
PDI	Protein disulfide isomerase
Pc	Pericentrin
shRNA	Small hairpin RNA
SP	Signal peptide
SR	Spectrin repeat
TPR	Tetratricopeptide repeat
WB	Western blot
WT	Wild type

Electronic supplementary material The online version of this article (doi:10.1007/s00018-010-0535-z) contains supplementary material, which is available to authorized users.

M. Schneider · W. Lu · I. Karakesisoglou (✉)
School of Biological and Biomedical Sciences,
University of Durham, Durham DH1 3LE, UK
e-mail: iakowos.karakesisoglou@durham.ac.uk

M. Schneider · S. Neumann · A. A. Noegel
Center for Biochemistry, Center for Molecular Medicine Cologne (CMMC), Cologne Excellence Cluster on Cellular Stress Responses in Aging-Associated Diseases (CECAD), Medical Faculty, University of Cologne,
50931 Cologne, Germany

A. Brachner · J. Gotzmann
Max F. Perutz Laboratories,
Medical University of Vienna, 1030 Vienna, Austria

Introduction

The acquisition of asymmetry (i.e., polarization) is a fundamental process exhibited by all living organisms. In metazoa, cell polarization is a prerequisite for directed cellular movement, tissue development, and homeostasis. In response to extracellular cues, cells align external and internal cellular structures towards the stimulus. Reorientation of the centrosome, Golgi apparatus, cytoskeleton, and nucleus enables cells to acquire the necessary geometry and sustains directional movement [1, 2].

Members of the evolutionarily conserved KASH (Klarsicht, ANC-1, and Syne1 homology) domain family, which includes the integral nuclear membrane proteins Kms1 in *S. pombe*; interaptin in *D. discoideum*; ANC-1, UNC-83, and ZYG-12 in *C. elegans*; Klarsicht and MSP-300 in *D. melanogaster*; syne in *D. rerio*; and the four mammalian nesprins, play pivotal roles in nuclear migration, centrosomal positioning, and consequently cell polarization [3–5]. KASH proteins positioned in the outer nuclear membrane function throughout evolution as adaptors that connect nuclei to surrounding cellular structures [4]. Kms1p, ZYG-12, and Klarsicht interact with dynein and mediate centrosome positioning and anchorage [6–8]. Nesprin-3 and nesprin-4 link intermediate filaments (IFs) and microtubule (MT)–associated structures, respectively, to the nuclear envelope (NE) [9, 10]. The largest 0.8–1 MDa expressed isoforms (termed giant: G) of the *syne-1/-2* (*Nesprin-1/-2*) loci in vertebrates tether nuclei to F-actin via their N-terminal actin-binding domain [11–13]. In addition, nesprin-2 isoforms containing the actin-binding domain interact with the ciliary membrane meckelin protein and mediate ciliogenesis [14].

The KASH-protein NE-targeting mechanism involves the C-terminal KASH domain, which interacts with inner nuclear membrane SUN-domain family members in the perinuclear space. These physical bridges (termed the "LINC" complex) span both nuclear membranes and link the cytoskeleton to the nuclear lamina [4, 15–17]. The lamin A/C–associated sun1/sun2-protein complexes are prerequisites for the proper nesprin NE anchorage [15, 16], as nesprin NE localization is affected when the underlying lamin meshwork is compromised [18–20]. Lamin A/C mutations themselves cause severe degenerative disorders (laminopathies), including muscular dystrophies and premature ageing [21, 22]. Moreover, lamin A/C functions are required for centrosomal tethering, cytoskeleton architecture, cellular mechanical stiffness, and cell polarity [23–26]. Consequently, cell polarization and centrosome positioning are the result of a trans-compartmental molecular connection, although the underlying molecular mechanisms remain elusive.

Similar to other NE proteins, nesprins are also involved in human degenerative disorders. Nesprin-1 mutations cause cerebellar ataxias, dilated cardiomyopathy, and arthrogryposis, whereas other nesprin-1/-2 mutations lead to muscular dystrophies [27–29]. Likewise, mice lacking the nesprin-1 C-terminal KASH domain exhibit a neuromuscular and a cardiac pathology [30]. Nesprin-2 giant isoform knockout mice (Nesprin-2 G−/−) are viable, exhibit an increased epidermal thickness, and harbor cell polarity defects [31]. In sharp contrast, the deficiency of nesprin-1/-2 KASH-domain isoforms results in severe laminary brain defects, respiratory failure, and lethality [32, 33]. While this evidence underlines their functional significance, it remains unclear why defects in these NE proteins have devastating degenerative effects in affected organisms.

Here, we characterize novel nesprin-2 associations with the kinesin-1 MT-motor protein apparatus. The plus-end-directed kinesin-1 motor comprises two kinesin heavy chains (KHCs) containing the motor domain and two light chains (KLC) providing cargo binding via their tetratricopeptide-repeat (TPR) domains [34, 35]. By associating directly with the TPR domains, nesprin-2 recruits KLC1 to the nucleus. These molecular frameworks require the linkage to an intact nuclear lamina in order to facilitate centrosome tethering, cytoskeleton organization, and cell polarization. By unravelling nesprin-2 as a key determinant of crucial cytoskeleton-associated processes that entail tissue morphogenesis, we provide novel insights into why NE defects are detrimental in vertebrates.

Materials and methods

Plasmid and shRNA construction

All cloned fragments were sequenced in their entirety. Constructs were tagged with myc, GFP, GST, Gal4-AD, Gal4-DNA-BD, or V5 by cloning the specific PCR fragment in frame into pCMV-Myc, pEGFP-C2 (Clontech), pGEX-4T-1 (Amersham), pGADT-7-Rec, pGBKT-7 vectors (Clontech), or pTracer^{TM}-EF/Bsd-B (Invitrogen), respectively. pcDNA3.1 (−) (Invitrogen) was used to engineer the DN-SUNL and the specific control (^{SP}GFP) constructs, which contain the torsin-A signal peptide (SP) sequence (MKLGRAVLGLLLLAPSVVQAV) at the N-terminus. All plasmids used and precise details of construction are indicated in supplementary material Table S1. Human KLC1 and nesprin-2 knock-downs were accomplished by plasmid-based RNA-interference (RNAi) as described [31]. All shRNA oligonucleotides were annealed and cloned into BseRI and BamHI sites of pSHAG-1 [36]. The following shRNA oligonucleotides were used: nesprin-2 C-terminal

shRNA, sense: 5′ gagaagaaactcaaacagtgaagcttgactgtttgag tttcttctcttttttt 3′, anti-sense: 5′ gatcaaaaaagagaagaaactcaaa cagtcaagcttcactgtttgagtttcttctccg 3′; nesprin-2 C-terminal control shRNA: sense: 5′ atctactcgacgtgagcgtgaagcttgac gctcacgtcgagtagatttttt 3′, anti-sense: 5′ gatcaaaaaatctactc gacgtgagcgtcaagcttcacgctcacgtcgagtagatcg 3′; nesprin-2 G shRNA [31]: sense: 5′ aaccagaagatgtggatgttgaagcttgaac atccacatcttct 3′, anti-sense: 5′gatcaaaaaaccagaagatgtggatg ttcaagcttcaacatcca 3′; KLC1 shRNA: sense: 5′ cagggtcttgaca atgttcacgaagcttggtgaacattgtcaagaccctgtttttt 3′, anti-sense: 5′ gatcaaaaaacagggtcttgacaatgttcaccaagcttcgtgaacattgtcaagacc ctgcg 3′; lamin A/C siRNA (Qiagen; [37]): target sequence: 5′ ggacttccagaagaaca 3′; lamin A/C control siRNA (Ambion; Silencer® negative control #1 siRNA)

Cell culture, transfection, MT depolymerization, and wounding assays

HaCaT, COS7, and NIH-3T3 cells were cultured at 37°C, 5% CO_2 in Dulbecco's Modified Eagles Medium, high glucose supplemented with 10% fetal calf serum, 2 mM penicillin, and 2 mM streptomycin (all from Sigma). For the cultivation of stable transfected DN-SUNL HaCaT cells, 0.5 mg/ml G418 disulfate (Sigma) was added to the nutrient solution. COS7 cells were transiently transfected at 170 V, 950 µF using a Gene-Pulser®II (Bio-Rad). For transient transfections of HaCaT and NIH-3T3 cell lines, the Amaxa Cell Line Nucleofector®Kit V (Lonza) was utilized. To depolymerize the MTs, 12.5 µM colchicine (Sigma) was added to the culture medium. HaCaT and COS7 cells were treated for 4 h, whereas NIH-3T3 cell lines were incubated for 2 h with colchicine before the fixation. Alternatively, MTs were depolymerized by incubating cells on ice for 30 min. To study cell polarization defects, confluent serum-starved HaCaT monolayers were wounded by scraping cells away with a P200 pipette tip. Cells were fixed 6 h after wounding and serum addition.

Immunofluorescence microscopy

Cells were fixed in 4% paraformaldehyde/phosphate-buffered saline (PBS) for 15 min and permeabilized in 0.5% Triton X-100/PBS for 4 min before the samples were processed for indirect immunostaining. To visualize intact MTs, cells were fixed with 4% paraformaldehyde/BRB80 (80 mM Pipes, 1 mM EGTA, 1 mM $MgCl_2$, pH 6.8) for 15 min, or alternatively with methanol for 10 min at −20°C. In wash-out experiments, cells were permeabilized in 0.1% Triton X-100/PBS for 10 s before the fixation. Nuclei were stained with 4,6-diamino-2-phenylindone (DAPI; Sigma) and F-actin with FITC-Phalloidin (Sigma). All indirect immunofluorescence samples were analyzed by confocal laser-scanning microscopy using either a TCS-SP1, a TCS-SP5 (Leica), or a LSM510 Meta Axiovert (Zeiss) with the exception of Fig. 4d, d′ and supplement Fig. S2, which were documented using the wide-field epifluorescence microscope DMR and a DC 350 FX camera (Leica).

Antibodies

Primary antibodies used were directed against the N-terminus of nesprin-2 (Nes2NT) mAb K56-386 [31] and mAb K20-478 [12], the C-terminus of nesprin-2 (Nes2CT) pAb K1 [19], γ-tubulin mAb GTU and β-actin mAb AC-74 (Sigma), pericentrin pAb Pc-4448 (Abcam), Myc mAb 9E10 [38], Sun1 pAb Sun1B and Sun2 pAb Sun2 [17], V5 mAb V5 (Invitrogen), GST pAb GST [39], GFP mAb K3-184-2 [40], KLC1 pAb H-75 (Santa Cruz), KLC1 mAb 63-90 (kind gift from Prof. Dr. S.T. Brady), KHC mAb H2 (Chemicon), tubulin mAb WA3 (kind gift from Dr. U. Euteneuer), Golgi mAb Gm130 (BD Transduction Laboratories), pan-keratin mAb AE1/AE3 (Milipore), PDI (Stressgen Biotechologies), and lamin A/C mAb Jol2 (kind gift from Prof. Dr. C.J. Hutchinson). For indirect immunofluorescence studies, Alexa 488, Alexa 568, and Alexa 647 fluorescently conjugated secondary antibodies (Invitrogen) were utilized. Peroxidase-coupled secondary antibodies (Sigma) were adopted in Western blot analysis.

Yeast two-hybrid analysis

The Matchmarker two-hybrid system 3 was adopted on the basis of the yeast protocols handbook (http://www.clontech.com/images/pt/PT3024-1.pdf; PT3024-1, Clontech). N2-SR was cloned into the yeast pGBKT-7 plasmid [19]. The Gal4-BD-N2-SR fusion was nontoxic and did not provoke autonomous activation. This bait was used in AH109 yeast to screen a pretransformed human brain cDNA library prepared in the pGADT-7-Rec expression vector, which generates Gal4-activating domain (AD)-cDNA fusion products in Y187 yeast (http://www.clontech.com/images/pt/PT3183-1.pdf; PT3183-1, Clontech). Positive AD-library plasmid DNA clones were isolated, sequenced, and retransformed with the N2-SR bait to confirm interactions.

Purification of GST-proteins, GST-pulldown assays, immunoprecipitation, and Western blotting

GST-fusion purification and GST-pulldown experiments were performed as described [19]. GST fusions were bound to Glutathione-Sepharose™ 4B (Amersham) at 4°C overnight. GFP-N2-SR-transfected or GFP-KLC1-transfected COS7 cell lysates were prepared using lysis buffer [50 mM Tris/HCl (pH 7.5), 150 mM NaCl, 1% Nonidet-P40, 0.5% sodium desoxycholate, and protease inhibitors (Roche)].

Lysates were then incubated with equal amounts of GST-fusion proteins coupled to GST-Sepharose beads at 4°C overnight. Samples were centrifuged, and the pellets were washed several times with PBS. Supernatants and pellets were assessed by SDS-polyacrylamide-gel electrophoresis (SDS-PAGE) [41], Coomassie Blue staining, and/or Western blot analysis [42].

Six-day-old mice brains were dissected out, submerged, and homogenized in lysis buffer or IP buffer (50 mM Tris/HCl (pH 7.5), 75 mM NaCl, 5 mM EDTA, 5 mM N-ethylmaleimide, 10 mM CHAPS, and protease inhibitors; adopted from [43]). Samples were centrifuged at 3,000*g* at 4°C for 20 min. The supernatants were processed through a 27-gauge needle (10 times), centrifuged at 12,000*g*, and employed for GST-pulldown analysis (see above) and immunoprecipitation.

For immunoprecipitation, analysis supernatants were pre-cleared with Protein-A-Sepharose CL-4B (Pharmacia Biotech) for 2 h at 4°C. Tissue samples were centrifuged for 1 min at 4°C and 1,000*g*. Supernatants (Input) were mixed with the specific purified antibodies (each 6 µg) and incubated for 4 h at 4°C. Protein-A-Sepharose beads were added to the antibody-antigen complexes, and the samples were incubated overnight at 4°C. Immunocomplexes were washed three times with PBS supplemented with protease inhibitors and subjected to SDS-PAGE concomitant with silver staining [44] and immunoblotting.

Densitometric measurements were performed using Image Gauge software (Version 4.23). Actin chemiluminescence signals provided standardized baselines.

Proteinase K digestions

HaCaT cells were transiently transfected with ^{SP}GFP and DN-SUNL constructs. Plates reaching 60–70% confluency were washed with ice-cold PBS, and the cells were removed from the plates by scraping. Cells were pelleted briefly by centrifugation at 1,000*g* and resuspended either in lysis buffer (see above) or in ice-cold hypotonic buffer [10 mM HEPES (pH 7.5), 1.5 mM $MgCl_2$, 1.5 mM KCl and 0.5 mM dithiothreitol]. Samples containing lysis buffer were incubated for 15 min on ice, centrifuged at 12,000*g*, and the supernatants were mixed with sample buffer. Cells resuspended in hypotonic buffer were either directly permeabilized with 5 µg/ml digitonin or 1% Triton X-100 for 4 min on ice before the samples were subjected to proteinase K (5 µg/ml) digestion for 30 min on ice. After the digestion, the lysates were supplemented with 10 µg/ml phenylsulfonyl fluoride (PMSF), centrifuged, and the supernatants incubated with sample buffer. Cell extracts were processed through a syringe, subjected to SDS-PAGE, and analyzed by Western blotting.

Statistical analysis

Statistical analysis was performed using Student's *t* test; 300 cells were used for every data set. Results were shown as mean ± SD. *P* values of ≤ 0.05 were considered significant. The mean ± SEM centrosome–nucleus distance was measured by the image processing software LAS AF (Leica Application Suite; Advanced Fluorescence Lite) and Zeiss LSM510 Image Browser.

Results

Nesprin-2 KASH proteins mediate centrosome attachment to the NE

To explore how nesprin-2 G (also known as NUANCE; [12]) controls cell polarization [31], we examined its functions in centrosome positioning and cytoarchitecture. We employed preferably HaCaT keratinocytes and COS7 cells due to their high expression of nesprin-2 G [19, 20]. Since the *syne-2* locus generates several structurally distinct isoforms, our studies also aimed to identify the implicated domains. In order to establish roles for KASH-domain-containing isoforms, we overexpressed the Sun1 luminal domain in the endoplasmic reticulum (ER) and perinuclear space, thereby achieving a saturation of KASH-domain binding sites. This was accomplished by fusing an ER signal peptide (SP) to the entire GFP-tagged Sun1 luminal domain (termed DN-SUNL, Fig. 1a). A fusion of SP to GFP alone was used as a control (^{SP}GFP, Fig. 1a). To confirm the proper translocation of SP fusions into the ER lumen and the perinuclear space, cell homogenates were subjected to proteinase K degradation in the presence of Triton X-100 or digitonin (Fig. 1b). In contrast to Triton X-100, which permeabilizes all biological membranes, low concentrations of digitonin leave the internal ER and NE membranes unperturbed. Similar to the ER and perinuclear space resident disulfide isomerase (PDI) protein, the ^{SP}GFP and DN-SUNL molecules were susceptible to proteinase K degradation only when cell homogenates were permeabilized with Triton X-100 (Fig. 1b).

The overexpression of ^{SP}GFP in HaCaT cells did not have any discernable effects on the nesprin-2 localization pattern (Fig. 2a′) or centrosome positioning (Fig. 2a″, arrow). In contrast, DN-SUNL functionally displaced nesprin-2 from the NE (Fig. 2b′, arrows). Furthermore, centrosome and Golgi polarization upon wounding was largely impaired (Fig. S1). This indicates that cellular asymmetry is affected when the physical linkage of outer nuclear membrane structures (KASH-protein interactomes) to SUN proteins is compromised. In addition, these mutants exhibited substantial centrosome positional changes with

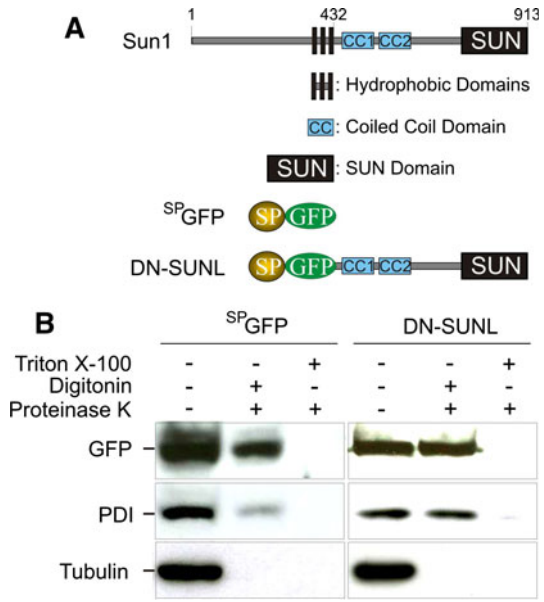

Fig. 1a, b The ^{SP}GFP and DN-SUNL fusions are targeted to the ER lumen and perinuclear space. **a** Schematic indicating the domain architecture of full-length Sun1, ^{SP}GFP, and DN-SUNL molecules. **b** Immunoblot analysis of cell homogenates expressing ^{SP}GFP and DN-SUNL, which were subjected to proteinase K treatment after digitonin or Triton X-100 permeabilization. Untreated cell lysates serve as positive controls. Note that in the presence of digitonin, the GFP fusions and the ER-lumen resident PDI protein resist proteinase-K-induced protein degradation, whereas tubulin is fully degraded. Complete degradation of the ^{SP}GFP and DN-SUNL proteins is achieved after Triton X-100 exposure

respect to the NE (Fig. 2b″, arrows). In control cells, centrosomes were positioned near the NE at a mean distance of 1.66 ± 0.12 μm, whereas a significant dislodgement was observed in two independent DN-SUNL-expressing clones, with an increase to 2.55 ± 0.23 μm ($P_{\text{DN-SUNL\#1}} = 3.56 \times 10^{-4}$) and 2.50 ± 0.20 μm ($P_{\text{DN-SUNL\#2}} = 5.71 \times 10^{-4}$), respectively (Fig. 2e).

The specific role of nesprin-2 G was investigated by silencing studies using shRNAs directed against the actin-binding domain (Fig. 2c). Consistent with our previous results, the average centrosome–NE distance increased significantly in nesprin-2 G–silenced cells (3.63 ± 0.21 vs. 1.52 ± 0.07 μm in control cells) (Fig. 2c, arrows, and Fig. 2e; $P_{\text{RNAi}} = 1.93 \times 10^{-17}$). A similar increase was found in primary fibroblasts obtained from nesprin-2 G−/− mice (Fig. 2e; $P_{-/-} = 3.56 \times 10^{-4}$). Intriguingly, the expression of a myc-tagged KASH-deficient C-terminal nesprin-2 fragment (termed N2-SR; Fig. 3a) recapitulated the centrosomal detachment phenotype (Fig. 2d). The mean centrosome–NE distance increased from 1.78 ± 0.10 μm in myc-transfected control cells to 3.30 ± 0.31 μm in N2-SR transfected cells (Fig. 2e; $P_{\text{myc-N2-SR}} = 6.74 \times 10^{-6}$). Collectively, these data unravel novel roles for nesprin-2 isoforms containing the actin-binding domain, KASH domain, and/or N2-SR domain in centrosomal anchorage.

In order to provide additional evidence for a function of nesprin-2 KASH isoforms in centrosomal positioning, we stained cells for the nesprin-2 KASH-domain binding proteins, Sun1 and Sun2 (Fig. 2f–f″, g–g″). Endogenous Sun1 did not form noticeable accumulations near centrosomal structures (Fig. 2f′, arrowhead, and Fig. 2f″, inset). Sun2, however, was found localized in distinct structures that lay in close proximity to the centrosome (Fig. 2g′–g″, inset). While the Sun2 presence at the centrosome attachment site confirmed previous findings [45], Sun1 only accumulated around the centrosome upon ectopic overexpression (data not shown). This result was further supported by our finding that RNAi-mediated knock-down of Sun2 also resulted in a significant centrosome detachment from the nuclear periphery (data not shown). Thus, these results suggest the presence of specific nesprin-2/Sun2-based macromolecular assemblies that span the entire NE facilitating centrosomal attachment to the nucleus.

Nesprin-2 associates with KLC1

To gain insights into the centrosome tethering mechanism, the nesprin-2 C-terminal fragment N2-SR [19] was further investigated. Interestingly, myc-tagged N2-SR still localized along the NE (Fig. 3b) in transiently transfected cells, despite the fact that it lacked a KASH domain. Intrigued by its localization properties and its ability to dislodge the centrosome from the NE (Fig. 2d), we performed a yeast two-hybrid library screen, in order to identify N2-SR-associated proteins. Using a Gal4-DNA-binding domain (BD)-fused N2-SR as bait, we identified full-length KLC1 as well as shorter KLC1 segments (Fig. 3c, lower panel) as nesprin-2 binding partners. As indicated in Fig. 3c (upper panel) and in contrast to controls, yeast harboring the KLC1 segment 138–560 (TPR-domains) and the N2-SR bait grew under restrictive growth conditions and expressed β-galactosidase (β-gal). Thus, the KLC1 C-terminal TPR domains were sufficient to mediate the nesprin-2 association. By subdividing N2-SR into smaller segments (N2-SR 1 + 2, N2-SR 2 + 3, and N2-SR 3 + 4), the nesprin-2 binding domain to KLC1 was narrowed down to N2-SR 2 + 3 (Fig. 3d).

Nesprin-2/KLC1 binding sites were confirmed by GST-pulldown studies. We engineered and purified a series of different GST-KLC1 (Fig. 3e) and GST-N2-SR fusions (Fig. 3f); beads and GST alone were used as negative controls. Equal amounts of recombinant proteins were immobilized on glutathione-agarose and incubated with GFP-N2-SR-expressing (Fig. 3e) or with GFP-KLC1-expressing (Fig. 3f) cell extracts, respectively. The predicted sizes and the usage of equal quantities of

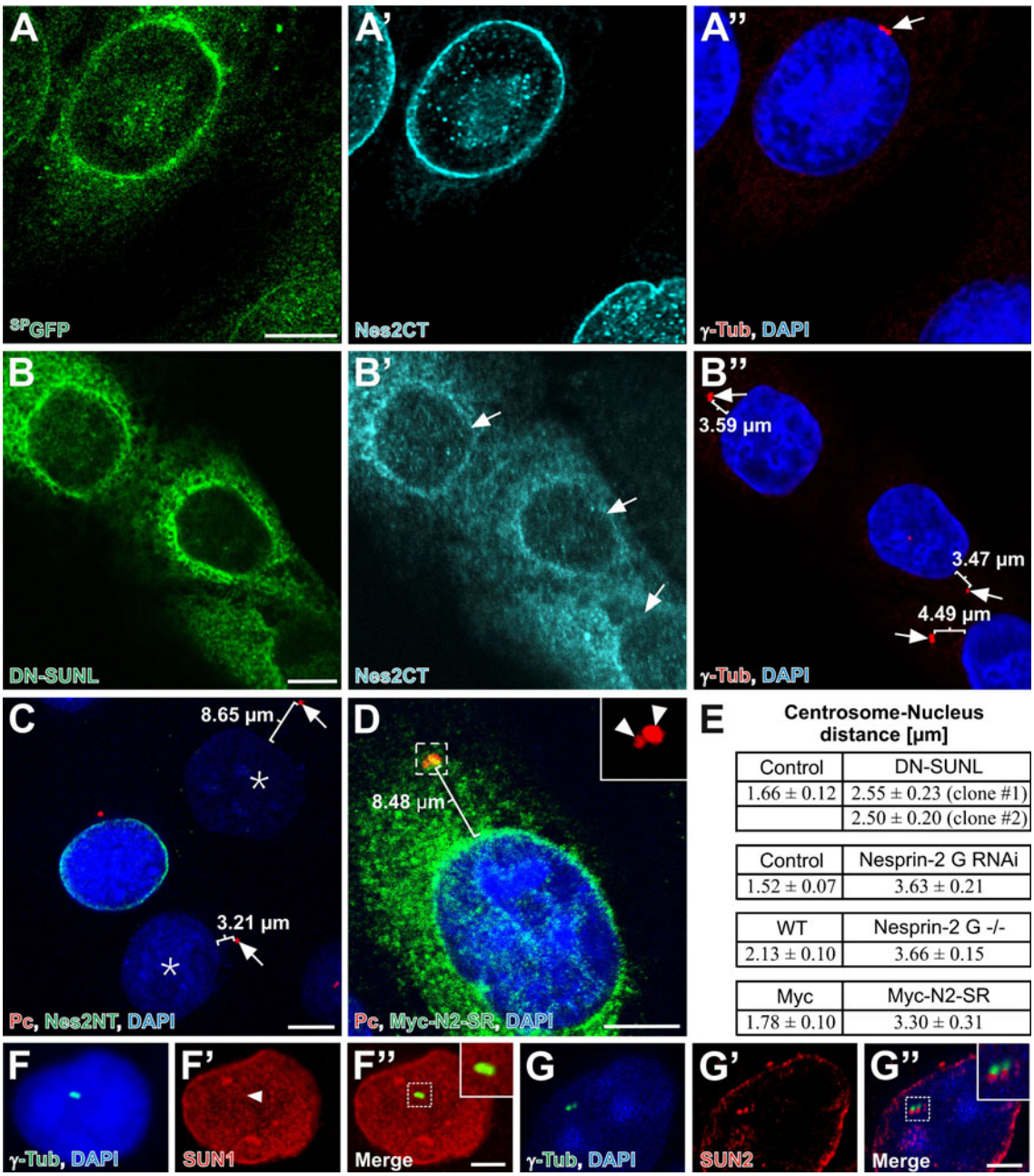

Fig. 2a–g Nesprin-2 KASH proteins tether the centrosome to the NE. ^{SP}GFP (**a**–**a**″) and DN-SUNL (**b**–**b**″) expressing HaCaT cells were subjected to indirect immunofluorescence using nesprin-2-specific (pAb Nes2CT) and centrosome-specific (γ-tubulin) antibodies. In contrast to the controls, mutants exhibit increased centrosome–nucleus distances (**b**″, *arrows*). See supplementary material Fig. S1 for DN-SUNL-induced cell polarity defects. **c** and **d** Nesprin-2 G–silenced HaCaT cells (*asterisks*) stained for pericentrin (pAb Pc) and nesprin-2 G (mAb Nes2NT) (**c**) as well as transiently transfected myc-N2-SR COS7 cells processed with pericentrin (**d**, *inset*, *arrowheads*) and myc antibodies (**d**) also show centrosomal detachment from the NE. *Scale bars* 10 µm. **e** Quantitative measurements of centrosome–nucleus distances in DN-SUNL, nesprin-2 G knockdown, nesprin-2 G knockout (−/−), myc-N2-SR-expressing, and control cells. Results are mean distances ± SEM. **f**–**g**″ HaCaT cells were stained for γ-tubulin and Sun1 (**f**–**f**″) or Sun2 (**g**–**g**″). Note that only Sun2 (**g**″) and not Sun1 (**f**″) accumulates underneath the centrosome. *Scale bar* 5 µm. DAPI was used to visualize DNA (**a**″, **b**″, **c**, **d**, **f**, **g**). *mAb* Monoclonal antibody, *pAb* polyclonal antibody

GFP-/GST-fusion proteins was verified by Western blotting or Coomassie staining (Fig. 3e–f). Immunoblotting on the precipitated samples demonstrated that the KLC1 interaction with nesprin-2 is mediated by the TPR domains and the N2-SR 2, N2-SR 2-3 segments, respectively. Notably, the strongest KLC1 binding was observed with N2-SR 2 + 3, which encompasses N2-SR 2 and N2-SR 2-3 (Fig. 3f). Moreover, we showed that KLC1 fusions that

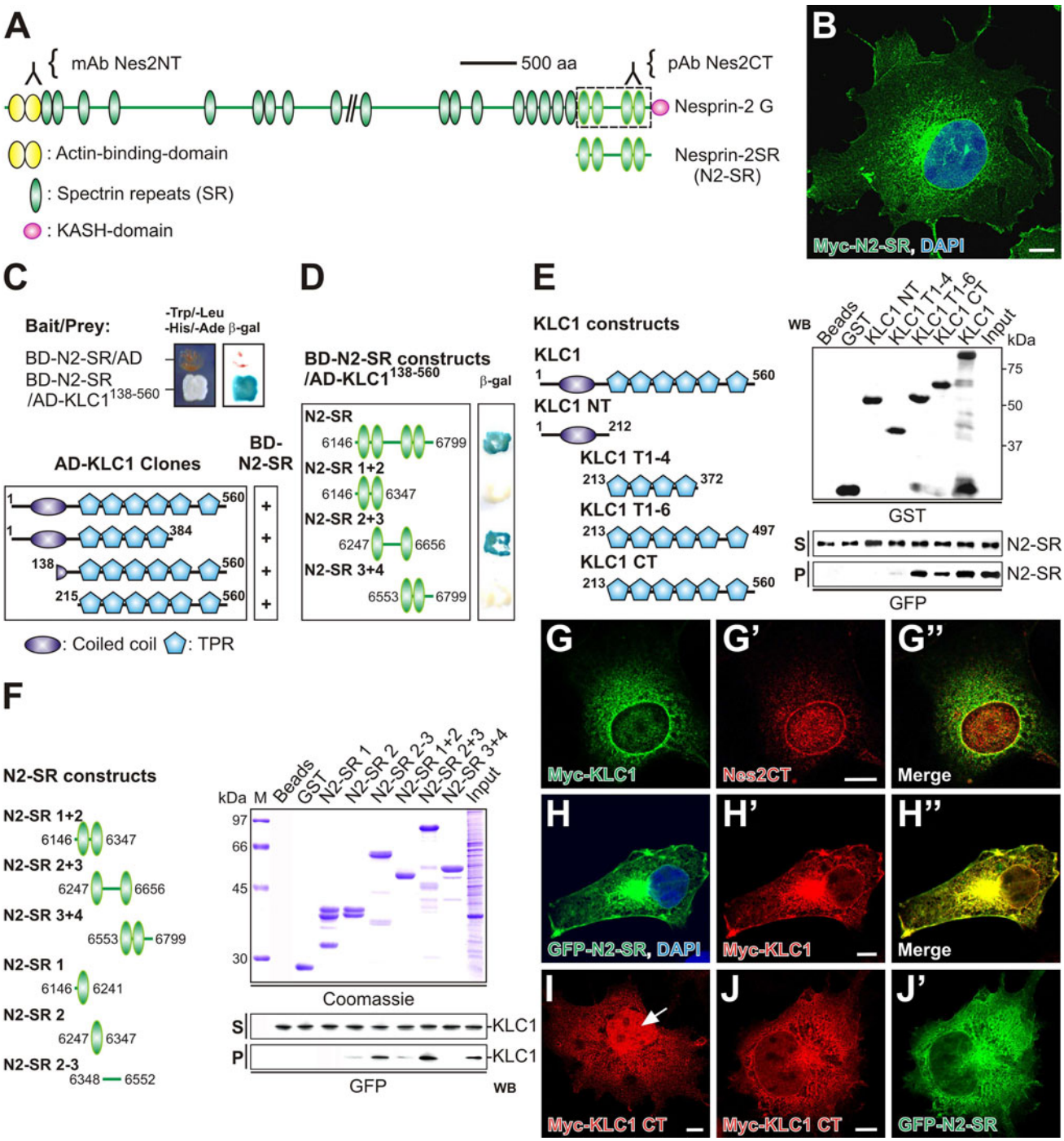

Fig. 3a–j Nesprin-2 interacts in vivo and in vitro with KLC1. **a** Illustration of nesprin-2 G and N2-SR structural features. N-terminal (NT) and C-terminal (CT) nesprin-2 antibody epitopes are marked (*inverted Y*). **b** Myc-tagged N2-SR-transfected COS7 cells were subjected to indirect immunofluorescence analysis using anti-myc-specific mAb. DNA was stained with DAPI. Note the N2-SR localization along the NE. **c** The yeast two-hybrid library screen yielded KLC1 as a new binding partner of N2-SR. Growth of BD-N2-SR and AD-KLC1$^{138–569}$ coexpressing AH109 yeast and the positive X-Gal assay indicates an interaction. Four independent BD-N2-SR-interacting AD-KLC1 clones could be identified in the yeast two-hybrid screen. **d** Mapping of the N2-SR-binding site by yeast two-hybrid analysis. **e** and **f** GST-pulldown analysis using different GST-tagged KLC1 (**e**) or GST-tagged N2-SR fusions (**f**) incubated with either GFP-N2-SR-transfected (**e**) or GFP-KLC1-transfected (**f**) COS7 cell extracts, respectively. *M* marker, *S* supernatant, *P* pellet, *WB* Western blot. **g**–**g**″ Myc-tagged KLC1 expressed in COS7 cells colocalizes with nesprin-2 at the nuclear rim. **h**–**h**″ GFP-N2-SR- and myc-KLC1-coexpressing COS7 cells stained with anti-myc mAb demonstrate colocalization. DNA visualized by DAPI stain. **i**–**j**′ Cells expressing either myc-KLC1 CT alone or GFP-N2-SR together with myc-KLC1 CT were stained with anti-myc mAb. Differential localization is indicated: nuclear staining (**i**, *arrow*), myc-KLC1 recruitment by GFP-N2-SR (**j**–**j**′). *Scale bar* 10 μm

harbor four TPR domains (T1–4) are sufficient to mediate nesprin-2 binding, although the association appeared weaker when compared to longer TPR fusions (Fig. 3e).

Further support of the interaction between nesprin-2 and KLC1 was found in COS7 cells ectopically expressing myc-KLC1 alone or in the presence of GFP-N2-SR. Immunofluorescence microscopy revealed intense myc-KLC1 staining at the NE, which colocalized with endogenous nesprin-2 in single transfected cells (Fig. 3g–g″). Interestingly, the KLC1 nuclear rim pattern remained unperturbed upon N2-SR co-expression. Moreover, the KLC1 and N2-SR fusions colocalized at the NE, cytoplasm, and cell periphery (Fig. 3h–h″). Intriguingly, the single transfected KLC1 C-terminal TPR domain fusions, KLC1 CT and KLC1 T1–6 (see Fig. 3e for construct details), localized unexpectedly in the nucleus (Fig. 3i, arrow). Upon N2-SR coexpression, however, these KLC1 fusions were excluded from the nuclear compartment and overlapped instead with N2-SR at the NE and in the cytoplasm (Fig. 3j–j′). Similar results were obtained in NIH-3T3 and HaCaT cell lines (data not shown). In summary these data corroborate the proposed interaction between the KLC1 TPR domains and nesprin-2 C-terminus.

Nesprin-2 forms complexes with the kinesin-1 motor protein apparatus

Inspired by the concentrated localization of overexpressed KLC1 at the nuclear rim, we next turned our focus to the biology of the endogenous KLC1 protein. In addition to its well documented pattern in the cytoplasm, endogenous KLC1 was strongly detected at the NE of HaCaT (Fig. 4a, arrowheads) and cerebellum cells, respectively (data not shown). Collectively, these data reveal the KLC1 NE localization as an authentic property of the endogenous protein.

Considering that KLC1 associates with KHC, we next investigated whether nesprin-2 is part of the kinesin-1 holoenzyme complex using GST-pulldown and coimmunoprecipitation assays. Equal quantities of the GST-tagged N2-SR 1 + 2, N2-SR 2 + 3, N2-SR 3 + 4, and N2-SR fusion proteins (see Fig. 3f for construct details) were used for precipitation of KLC from murine brain homogenates. These studies demonstrated the specific binding of N2-SR and N2-SR 2 + 3 to KLC1 and KHC (Fig. 4b, left panel). Comparable results were obtained when endogenous nesprin-2 was immunoprecipitated from mouse brain extracts and revealed the presence of various nesprin-2 isoforms, KLC1, KHC, and tubulin (Fig. 4b, right panel). Supportively, analysis of coexpressed myc-tagged KHC and GFP-KLC1 in COS7 cells exhibited qualitative colocalization with nesprin-2 along the NE (Fig. 4c, inset). Interestingly, the presence of KLC1 at the NE of COS7 and fibroblast cells coincided largely with the presence of prominent NE-associated MT structures (Fig. 4d and Fig. S2). In summary, these data suggest that nesprin-2 physically tethers the microtubule-based kinesin-1 motor protein complex to the outer nuclear membrane.

In order to examine whether the KLC1 NE localization depends on the MT network, transiently transfected GFP-KLC1 COS7 cells were immunostained for tubulin in the presence and absence of the MT-depolymerization drug colchicine (Fig. 4d, d′). Although the NE of cells treated with colchicine lacked intact MT structures, the GFP-KLC1 localization remained unaffected (Fig. 4d′). Thus we concluded that the KLC1 nuclear rim localization does not require an intact MT network.

KLC1 NE-targeting requires KASH/SUN protein interactions

Next we elucidated the involvement of lumenal KASH/SUN protein interactions into the KLC1 NE-targeting mechanism. Therefore, transiently transfected control (^{SP}GFP) and DN-SUNL NIH-3T3 fibroblasts were immunostained for nesprin-2 G and KLC1. Our decision to use this particular cell line model, as opposed to HaCaT cells, was based on the prevalence of nesprin-2 C-terminal KASH-domain isoforms in fibroblasts [31]. In sharp contrast to control cells (Fig. 5a, arrow), the DN-SUNL expression (Fig. 5b, asterisk) not only dislodged nesprin-2 from the NE but also KLC1 (Fig. 5b, arrows and Fig. 5b′). Importantly, nesprin-2, KLC1, tubulin, and actin expression levels remained unaffected upon DN-SUNL expression (Fig. 5b″). These data suggest that DN-SUNL affects the KLC1 topology by disrupting protein–protein interactions at the NE. Notably we also observed a direct correlation between the nesprin-2 and KLC1 NE staining intensities in untreated NIH-3T3 cells. Cells exhibiting weak nesprin-2 signal (Fig. 5c, asterisk) harbored reduced KLC1 staining, whereas brightly nesprin-2-stained cells also exhibited a strong KLC1 NE staining (Fig. 5c, arrows). Similar observations were noted between KLC1 and tubulin structures. Colchicine-treated cells exhibiting strong KLC1 NE staining consistently harbored intensive tubulin NE signals as well (Fig. 5c′, arrowhead) and vice versa (Fig. 5c′, arrow).

Nesprin-2 regulates the amount and the subcellular localization of KLC1

Using a silencing approach, we intended to define the hierarchy and physiological significance of the previously identified molecular players that tether KLC1 at the NE. HaCaT cells were transiently transfected with nesprin-2 G

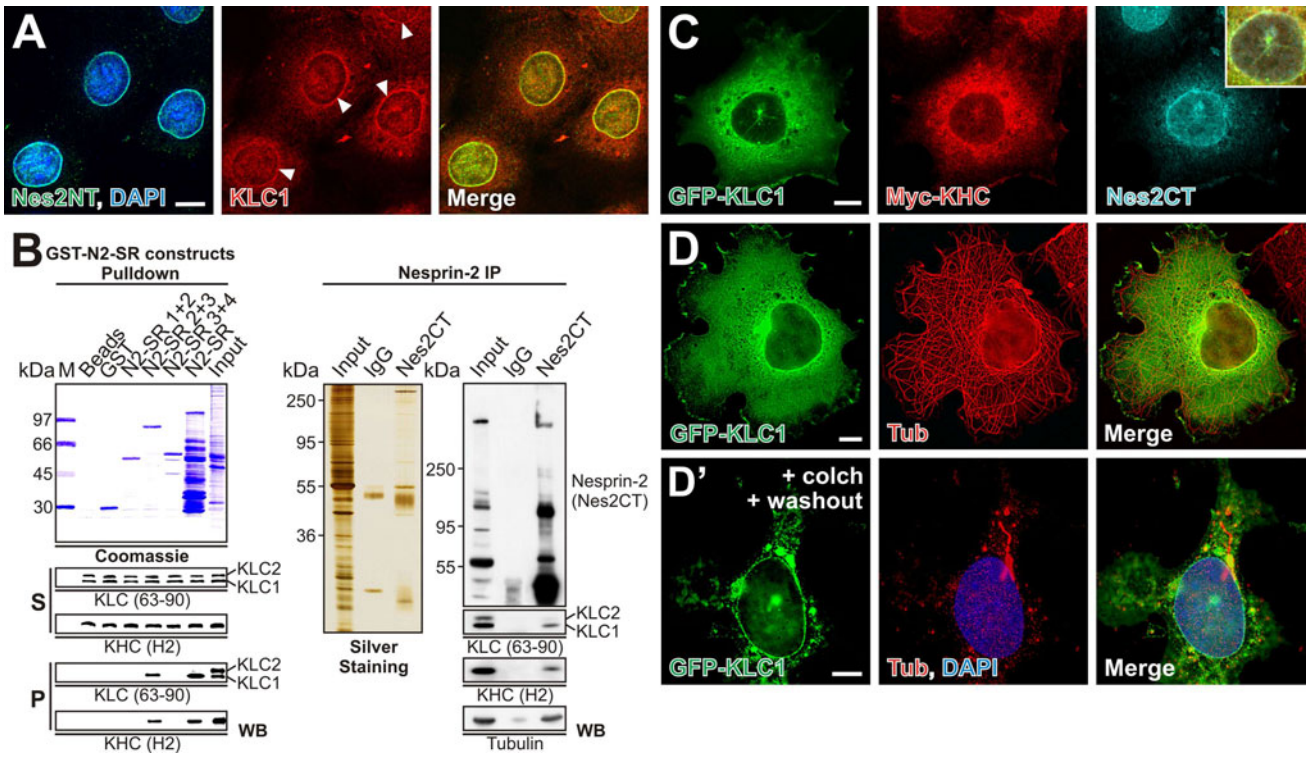

Fig. 4a–d Nesprin-2 associates with kinesin-1 at the NE. **a** Immunostainings of HaCaT cells using nesprin-2-specific (mAb Nes2NT) and KLC1-specific antibodies shows KLC1 along the NE (*arrowheads*), where it overlaps with nesprin-2. Nuclei are stained with DAPI. **b** GST-pulldown and immunoprecipitation (IP) were performed using GST-tagged N2-SR fusions and pAb Nes2CT, respectively. Precipitated brain lysates were separated on 12% SDS-PAGE stained with Coomassie (GST-pulldown, *left*) or on 3–15% SDS-PAGE gradient gels probed with pAb Nes2CT (*IP, right*). Silver staining was used as a control. **c** Cells transiently transfected with GFP-tagged KLC1 and myc-tagged kinesin heavy chain (KHC) were stained with specific myc and nesprin-2 (pAb Nes2CT) antibodies. Note KLC1, KHC, and nesprin-2 colocalization along the NE (**c**, *inset*). **d** and **d′** Untreated (**d**) and colchicine-treated, pre-extracted (**d′**) GFP-KLC1 expressing cells were subjected to indirect immunofluorescence using anti-tubulin mAb. DAPI visualizes nuclei. Tubulin is enriched at the NE in control cells (**d**), whereas in colchicine and pre-extracted cells nearly all tubulin structures are washed out (**d′**). Note that the GFP-KLC1 NE localization is unaffected in cells lacking MTs (**d′**). *Scale bars* 10 μm. See also supplementary material Fig. S2

shRNA constructs and stained for nesprin-2 G and KLC1. Upon silencing of nesprin-2 G we observed a lack of NE-associated KLC1 (Fig. 6a–a″, asterisks) and a distinct reduction of the KLC1 staining. Therefore we analyzed and compared the protein lysates of cells after KLC1 or nesprin-2 silencing. Whereas KLC1 silencing did not significantly alter the expression levels of nesprin-2, KLC1 protein levels were significantly reduced in the nesprin-2 knock-down lysates (Fig. 6b). Densitometric measurements on the Western blot signals (three independent experiments) indicated a 51% reduction in KLC1 expression when compared to untransfected HaCaT extracts. This observation was corroborated by an alternative silencing strategy that eliminated, in addition to nesprin-2 G, the C-terminal nesprin-2 isoforms (Fig. S3). Collectively these experiments show that KLC1 protein levels are tightly coupled to that of nesprin-2.

In order to investigate a potential role of nesprin-2 and KLC1 in the organization of perinuclear MTs, nesprin-2 G–silenced and KLC1-silenced HaCaT cells were examined under conditions that induce MT depolymerization. Nesprin-2-silenced cells exhibited the anticipated nuclear deformations (Fig. 6c, asterisk) and harbored diminished tubulin staining at the NE (Fig. 6c′, arrows) compared to untransfected cells (Fig. 6c′, arrowheads). Interestingly, pronounced MT structures, even resisting cold-induced MT depolymerization [46], were visible at the NE of untransfected HaCaT cells (Fig. 6d–d′, arrowheads) and were mostly associated with NE-localized KLC1. Hence we speculated whether KLC1 is directly involved in the organization of perinuclear MTs. Indeed, when KLC1 was silenced (Fig. 6e, asterisks), the MT network at the NE was strongly reduced (Fig. 6e′) compared to KLC1-positive control cells (Fig. 6e′, arrowheads).

Since lamin A/C affects the NE localization of nesprin-2, we next assessed the consequences of lamin A/C silencing on KLC1. In addition to dislodging nesprin-2 from the NE (Fig. 7b′, arrows), absence of lamin A/C led to a complete lack or only weak KLC1 NE staining (Fig. 7d′, arrows). Similar to DN-SUNL, the lamin A/C loss left the nesprin-2,

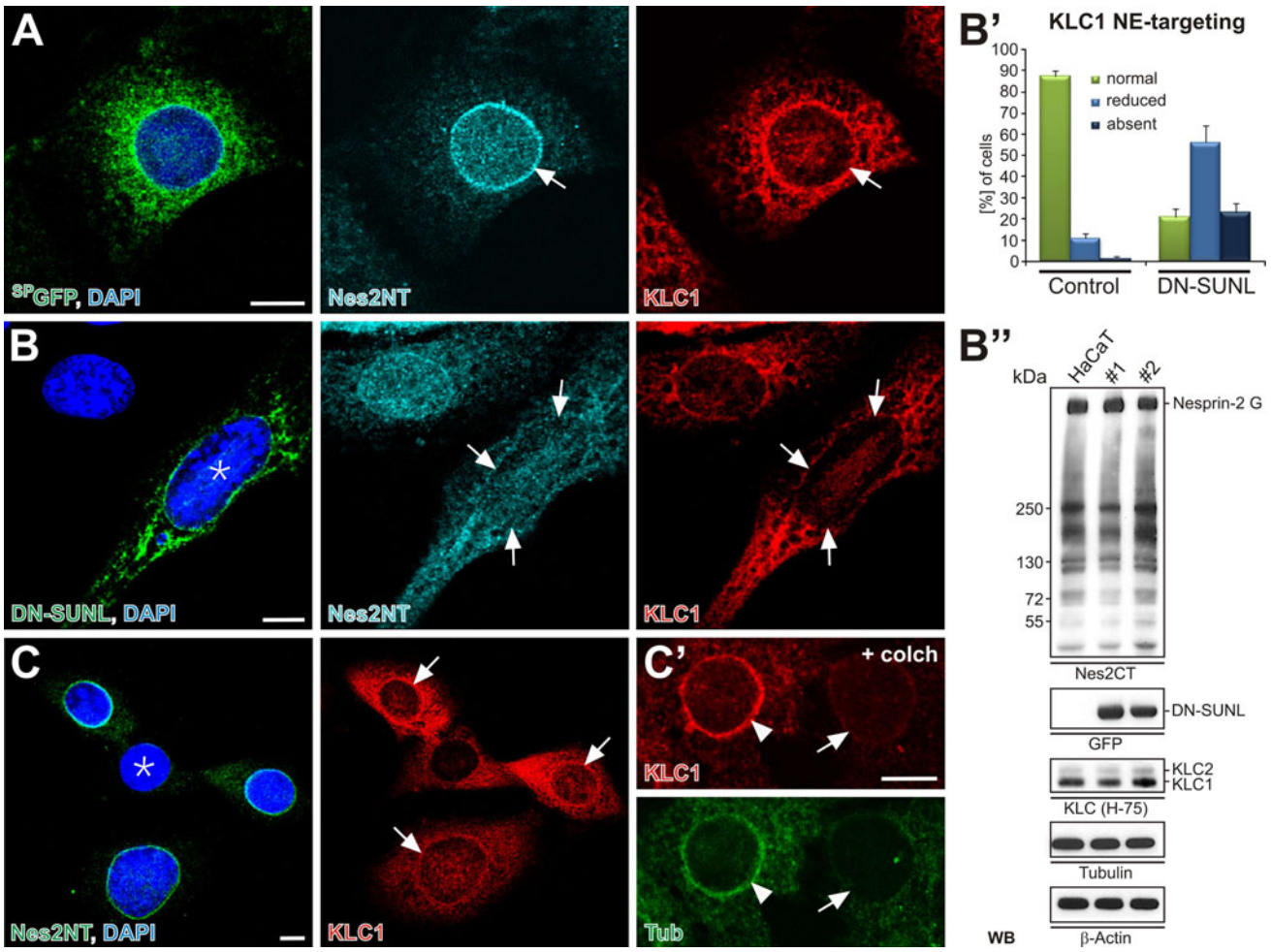

Fig. 5a–c SUN-protein dominant-negative (DN) interference affects KLC1 NE localization. NIH-3T3 fibroblasts transiently expressing ^{SP}GFP control (**a**) and DN-SUNL constructs (**b**) were subjected to indirect immunofluorescence using anti-nesprin-2 (Nes2NT, mAb K56-386) and anti-KLC1 (pAb H-75). The nesprin-2 and KLC1 NE pattern is unaffected in control fibroblasts (**a**, *arrows*). In DN-SUNL-expressing cells (**b**, *asterisk*), however, staining of both nesprin-2 and KLC1 NE is diminished (**b**, *arrows*). **b′** The histogram represents a statistical evaluation of the KLC1 localization phenotypes at the NE in control and DN-SUNL-expressing cells (results are the mean ± SD; Student's *t* test: $P_{normal} = 3.84 \times 10^{-4}$, $P_{reduced} = 6.46 \times 10^{-3}$, $P_{absent} = 1.79 \times 10^{-2}$). **b″** Immunoblot analysis of stably transfected DN-SUNL human keratinocytes (HaCaT; clones #1 and #2) and untransfected HaCaT control cells. Note that the DN-SUNL expression did not alter the nesprin-2, KLC1, and tubulin expression levels. Actin is shown as a loading control. **c** Untransfected NIH-3T3 fibroblasts exhibiting weak nesprin-2 staining (*asterisk*) have a decreased KLC1 immunostaining at the NE, whereas an intensive nesprin-2 signal correlates with strong KLC1 staining at the NE (*arrows*). DAPI was used to visualize DNA. **c′** KLC1 and tubulin stainings of colchicine-treated NIH-3T3 cells indicate a direct correlation of their fluorescence intensities at the NE (*arrows* denote weak staining signals, whereas strong signals are labelled by *arrowheads*). *Scale bars* 10 μm

KLC1, and tubulin expression levels unperturbed (Fig. 7e). In summary, these data suggest that an intact nuclear lamina enables nesprin-2 to recruit KLC1 and structure the MT cytoskeleton at the nuclear surface.

The KLC1 loss affects centrosome anchorage and cell polarization

Next we questioned whether the cellular phenotypes exhibited by nesprin-2 mutants (i.e., aberrant centrosomal positioning and cell polarization) arise via KLC1 deregulation. Silencing experiments in HaCaT cells indicated that, similar to nesprin-2, the loss of KLC1 caused centrosomal detachment from the NE (Fig. 8a–a′). Centrosomes were positioned 1.52 ± 0.07 and 4.09 ± 0.21 μm away from the NE surface, in control and mutant cells, respectively (Fig. 8b). Moreover, KLC1 downregulation resulted in defective cell polarization during wound healing in scratch assays (Fig. 8d). While in 97% of control cells the centrosome was positioned within a 120° area facing the wound (Fig. 8c), this number dropped to 45% in KLC1 knock-down cells (Fig. 8e). Taken together, these data demonstrate that KLC1 loss recapitulates major aspects of the nesprin-2 G mutant cellular phenotype.

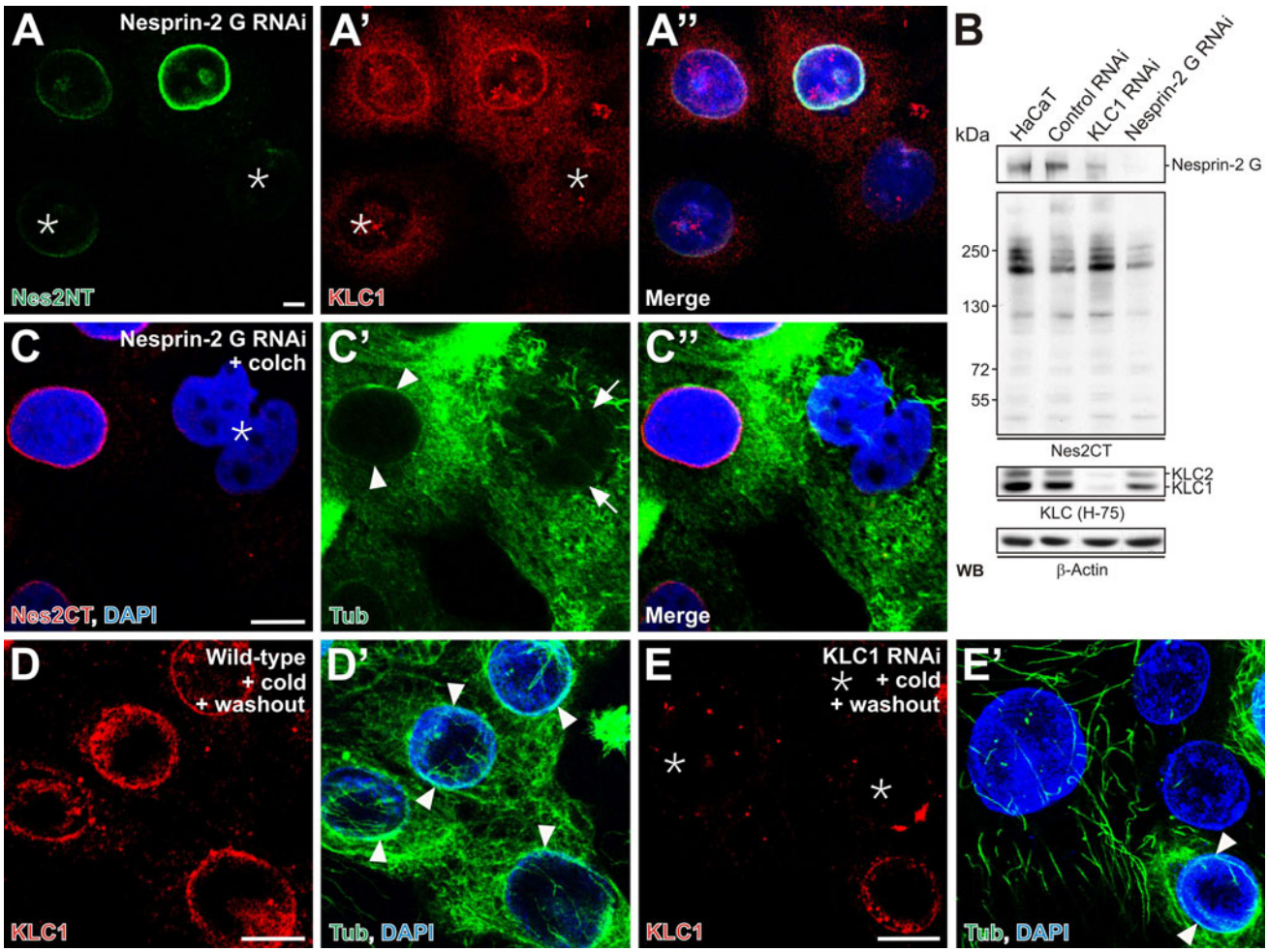

Fig. 6a–e Loss of nesprin-2 G alters expression and NE targeting of KLC1. **a**–**a**″ Immunostainings of nesprin-2 G–silenced cells (*asterisks*) using nesprin-2 G–specific (Nes2NT) and KLC1-specific antibodies. Nuclei are stained by DAPI. KLC1 NE staining is either reduced or absent in nesprin-2 G knock-down cells. **b** Western blot analysis of control, KLC1, and nesprin-2 G knock-down HaCaT homogenates indicates protein silencing efficacy. Note that nesprin-2 G loss affects KLC1 expression. **c**–**c**″ Nesprin-2 G knock-down and colchicine-treated cells (*asterisk*) stained for tubulin lack pronounced tubulin structures at the NE (**c**′, *arrows*). Nesprin-2-positive cells, however, show clear accumulation of tubulin along the NE (**c**′, *arrowheads*). **d**–**e**′ Control (**d**, **d**′) and KLC1-silenced (**e**, **e**′) cells were incubated on ice to depolymerize MTs. Detergent pre-extracted cells were fixed and stained for KLC1 and tubulin. Note that the existence of KLC1 at the NE is accompanied by the presence of MTs along the NE (**d**′ and **e**′, *arrowheads*). *Scale bars* 10 μm

Nesprin-2 determines cell architecture

Since centrosome polarization in wounded fibroblast monolayers is the result of actin-based nuclear movement away from the wound edge [47], we examined the perinuclear F-actin organization in nesprin-2-silenced cells. The presence of prominent F-actin perinuclear filaments (Fig. 9a, a′, arrows and insets) coincided with the occurrence of nesprin-2. These structures were largely absent in nesprin-2-silenced cells (Fig. 9b, arrowheads, insets, and Fig. 9c), which also exhibited profound stress fibers throughout their cytoplasm (Fig. S4). Examination of the intermediate filament (IF) network in WT cells revealed pronounced keratin bundles adjacent to the NE (Fig. 9d″, arrows and inset). Upon nesprin-2 depletion, however, these bundles were drastically reduced or absent from the NE (Fig. 9d″, arrowheads, and Fig. 9e). Frequently IFs were found a few micrometers away from the NE in nesprin-2 knock-down cells (Fig. 9d″, arrowheads, inset). In addition, nesprin-2 mutants displayed fragmented or perinuclear-arranged Golgi structures (Fig. 9f–g). Based upon these results we conclude that nesprin-2 exerts an integrative and essential function in organizing major cellular structures and organelles at the intersection between nuclear interior and cytoplasm.

Discussion

The NE and in particular the nuclear lamina have been spotlighted during the past decade in the scientific

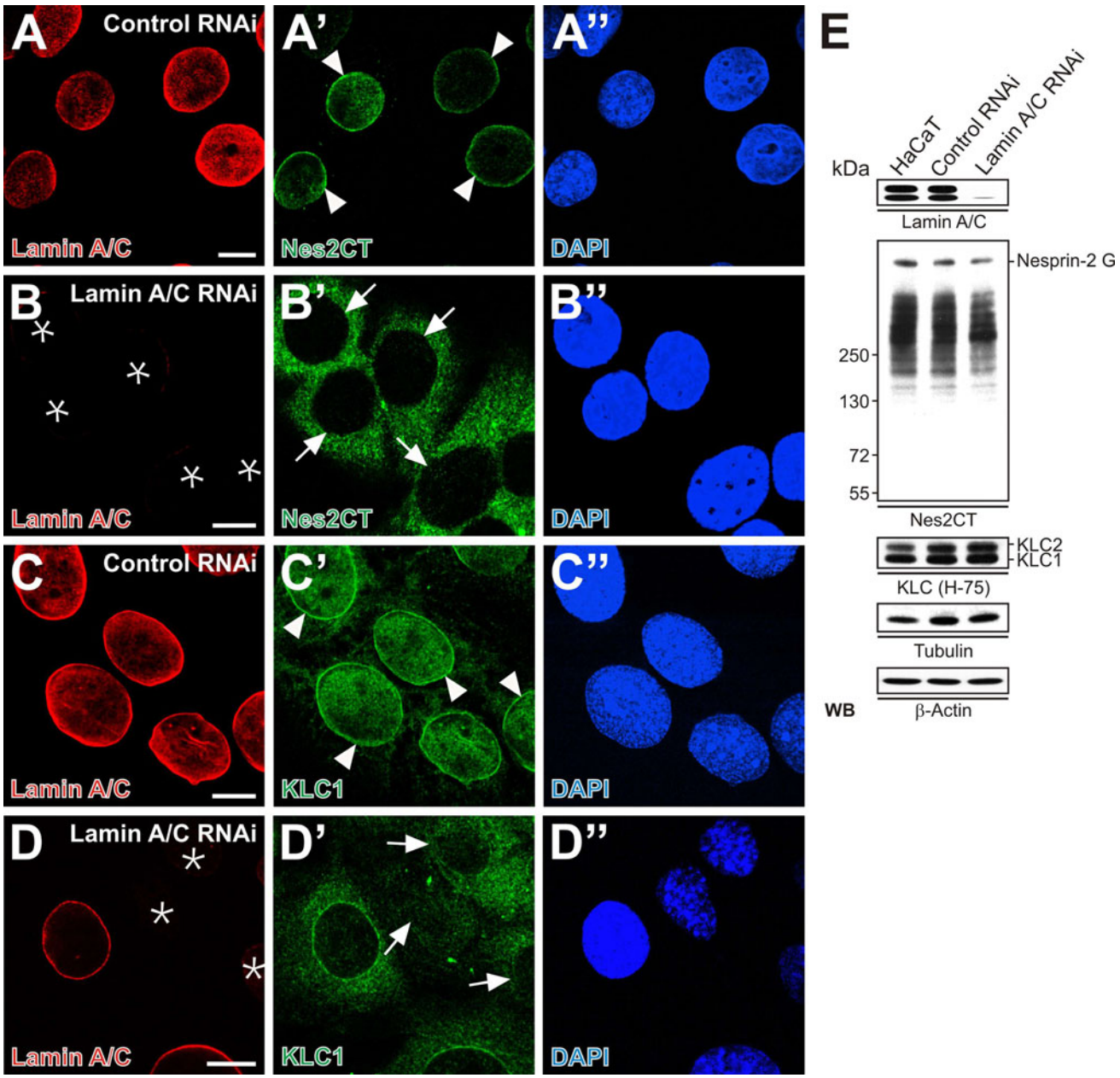

Fig. 7a–e Lamin A/C determines the localization of both KLC1 and nesprin-2 at the NE. HaCaT cells were transiently transfected with control (**a**–**a**″ and **c**–**c**″) or lamin A/C siRNAs (**b**–**b**″ and **d**–**d**″) and costained for lamin A/C and nesprin-2 (pAb Nes2CT) (**a**, **a**′ and **b**, **b**′) or lamin A/C and KLC1 (**c**, **c**′ and **d**, **d**′). While lamin A/C-positive control cells (**a**, **c**) exhibit prominent localization of nesprin-2 and KLC1 at the NE (**a**′, **c**′, *arrowheads*, respectively), in lamin A/C-silenced cells (**b**, **d**, *asterisks*) both nesprin-2 and KLC1 NE structures are either less pronounced or completely absent (**b**′, **d**′, *arrows*, respectively). **e** Immunoblot analysis of untransfected, transiently transfected control and lamin A/C RNAi HaCaT cell lysates

community due to the fact that an increasing number of mutations in those genes could be linked to a large and heterogeneous group of inherited diseases in humans, the so-called laminopathies. Their pathogenesis is currently explained by several nonmutually exclusive hypotheses [21, 22, 48]. Especially applicable for our new findings would be the "structural" hypothesis. It is based on the assumption that defects in the nuclear lamina compromise the NE structural integrity and render cells more susceptible to mechanical stress-induced cell degeneration. Indeed it could be shown that lack of lamin A/C results in reduced mechanical stiffness, which is determined by the LINC complex [25]. Additionally, impaired cytoskeletal organization, loss of cell polarity, and centrosomal mispositioning were described [23, 24, 26]. The underlying molecular mechanisms were, however, poorly understood.

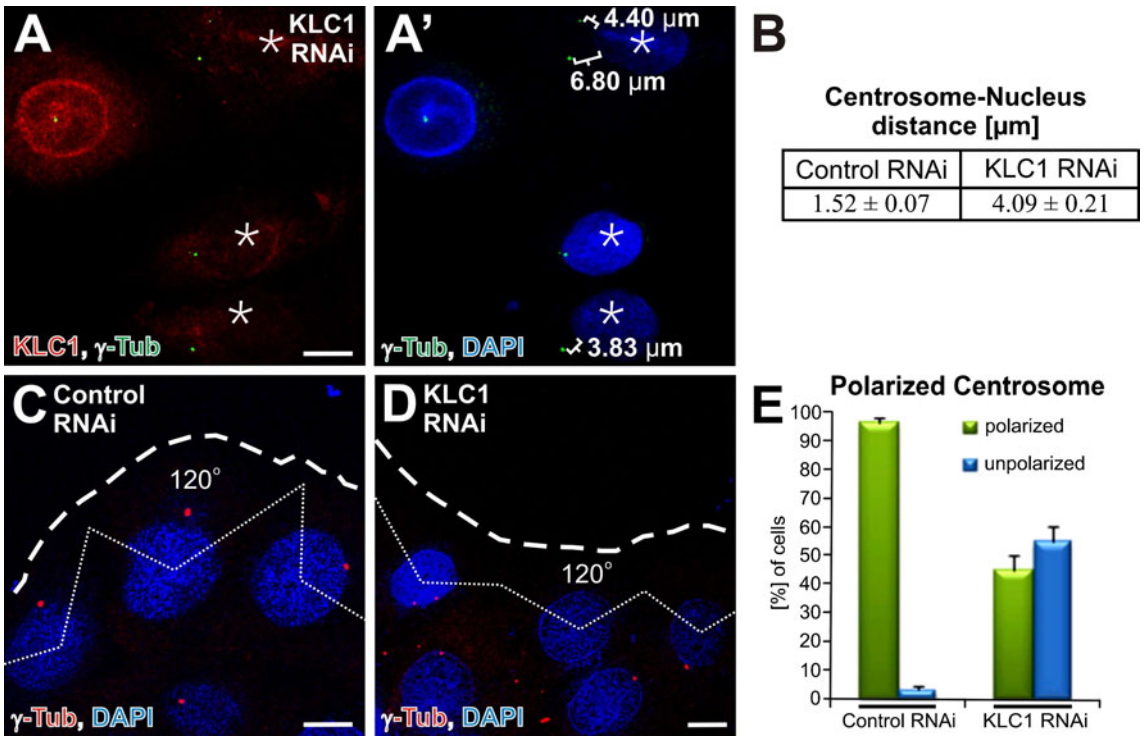

Fig. 8a–e KLC1 mediates centrosome anchorage and functions in cell polarity. **a** and **a′** KLC1 knock-down HaCaT cells (*asterisks*) stained for KLC1 and γ-tubulin exhibit increased centrosome–nucleus distances. Nuclei were stained with DAPI. **b** Statistical evaluation of control and KLC1-silenced cells illustrate a significantly (Student's *t* test: $P = 3.38 \times 10^{-26}$) increased centrosome–nucleus distance in KLC1 mutants. Values are mean distances ± SEM. **c** and **d** Indirect immunofluorescence examination of control (**c**) and KLC1-silenced (**d**) cell monolayers 6 h post-wounding using antibodies against γ-tubulin and KLC1. Nuclei were visualized with DAPI. The *dashed lines* indicate the wound edge. Note that the centrosomes are not positioned towards the leading edge when KLC1 is absent. **e** Statistical evaluation of the representative experiments shown in **c** and **d** indicates defective cell polarization upon KLC1 knock-down. Centrosomes positioned within a 120° sector (*dotted line*) facing the wound were assessed as polarized. Results are the mean ± SD; Student's *t* test: $P = 3.03 \times 10^{-3}$. *Scale bars* 10 µm

Our data now provide important mechanistic insights into these processes and offer clues that far-reaching forces interconnect larger cellular entities with the nuclear lamina.

A LINC subcomplex, which includes nesprin-2, KLC1, KHC, and MTs, is central to laminopathic cellular defects

We uncover here that nesprin-2 binds both in vitro and in vivo to the KLC1 C-terminal TPR domains and forms complexes with KHC and MTs at NE anchor points. Similar to other LINC complex constituents such as Sun2 and nesprin-2 [16, 19], the KLC1 nuclear rim localization required lamin A/C. Based on our data, we postulate that this effect is indirect and due to nesprin-2 mislocalization, considering that nesprin-2 silencing is sufficient to dislodge KLC1 from the NE. However, other NE constituents than nesprin-2 may also bind to KLC1 and strengthen this connection. Indeed it was shown recently that KLC can be recruited by UNC-83 and nesprin-4 KASH proteins [10, 49]. Our data on the KLC1 localization at the NE corroborates previous reports [50–52] and provides for the first time insights into the potential functions of KLC1 at the NE. We could show that NE-associated KLC1 organizes the perinuclear MT network. This function may directly account for the neurological pathologies observed in nesprin-1/-2 KASH-domain knockout animals [33, 53], considering that functional perinuclear MT "cages" are critical for neuronal migrations [54].

We have previously shown that nesprin-2 G controls cell polarization and cellular migration [31]. We now show that cellular asymmetry is also affected when the binding of KASH proteins to SUN proteins is interrupted or when KLC1 is silenced. Taking into account that similar cell polarity defects are triggered when lamin A/C is missing or mutated, this evidence suggests that the aforementioned proteins operate within the same structural and functional framework.

Nesprin-2 affects major cytoskeletal networks and Golgi structure

This study shows that nesprin-2 is involved in the organization of major cytoskeletal elements (i.e., MTs, IFs, and F-actin). By determining how nesprin-2 interacts with

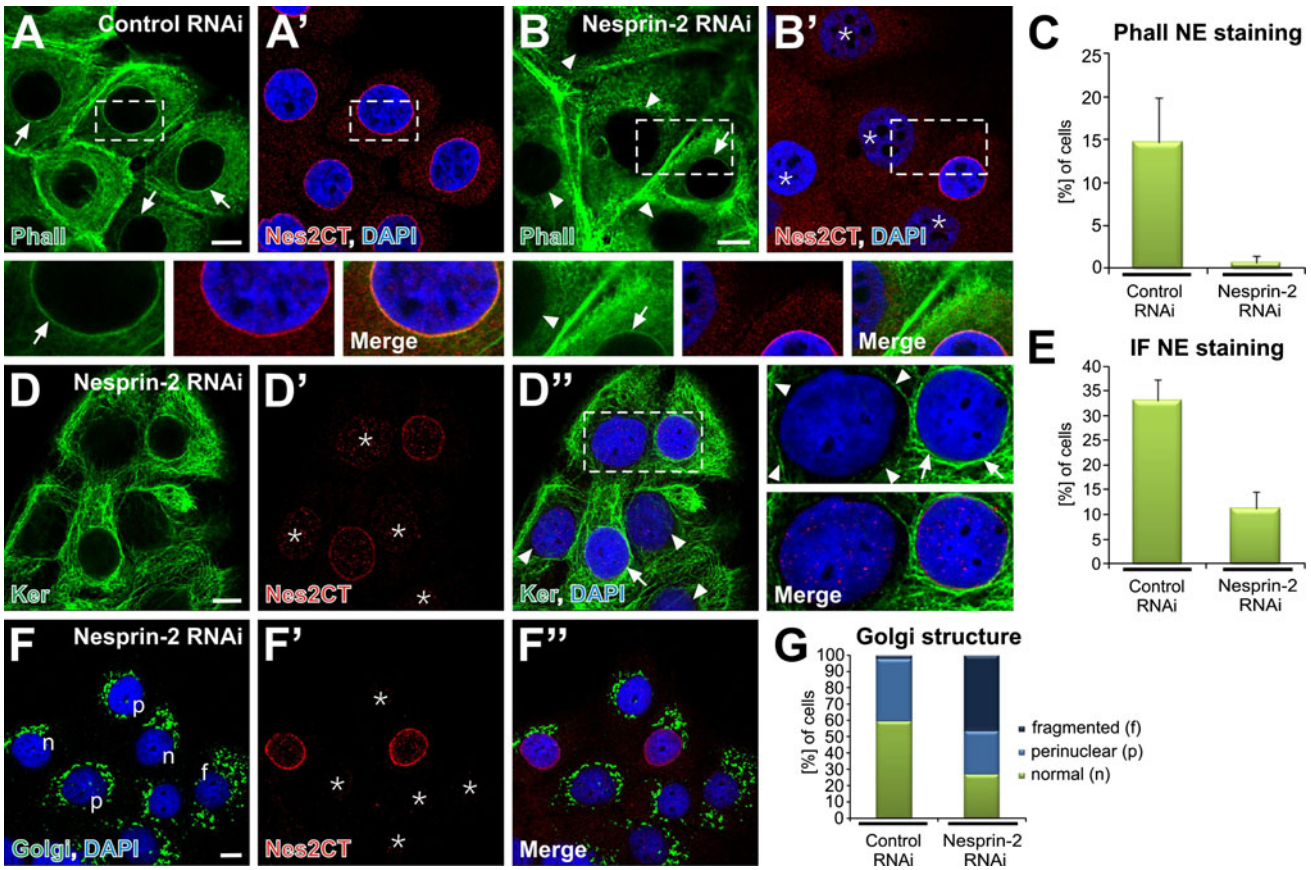

Fig. 9a–g Nesprin-2 controls cell architecture. **a**–**b**′ Control (**a**–**a**′) and nesprin-2-silenced (**b**–**b**′, *asterisks*) HaCaT cells were stained for nesprin-2 (pAb Nes2CT) antibodies and FITC-phalloidin (Phall). Nesprin-2-positive cells display F-actin-rich perinuclear structures (*arrows and insets*), which are lost from the NE of nesprin-2-deficient cells (*arrowheads and insets*). *Insets* are higher magnifications of the *boxed areas*. **c** Statistical evaluation of perinuclear F-actin structures in control and nesprin-2-silenced cells. Results are the mean ± SD, Student's *t* test: $P = 2.57 \times 10^{-3}$. See also supplementary material Fig. S4. **d**–**d**″ Indirect immunofluorescence examination of the keratin network in nesprin-2-silenced cells (**d**′, *asterisks*) indicates the absence of perinuclear IF structures (*arrowheads*). Note the presence of pronounced IF bundles at the NE of nesprin-2-positive cells (*arrows*, *insets*). Nuclei were visualized with DAPI. **e** Statistical evaluation of perinuclear IFs in control and nesprin-2-silenced cells. Results are the mean ± SD, Student's *t* test: $P = 2.57 \times 10^{-2}$. **f**–**f**″ Golgi apparatus immunostaining reveals fragmented (*f*) or perinuclear (*p*) arranged structures in nesprin-2-silenced cells (**f**′, *asterisks*) as compared to the confined Golgi cisternae arrangement (*n* normal) in nesprin-2-positive cells. **g** Quantification analysis reveals the occurrence of Golgi defects in nesprin-2 knock-downs. Results are the mean ± SD, Student's *t* test: $P_{(n)} = 1.89 \times 10^{-2}$, $P_{(p)} = 5.00 \times 10^{-2}$, $P_{(f)} = 1.80 \times 10^{-3}$. *Scale bars* 10 μm

kinesin-1, the effects on MTs can now be reasonably explained. Since nesprin-2 is an F-actin-binding protein [12], an impact on the perinuclear F-actin cytoskeleton was very likely, but intriguingly, loss of nesprin-2 coincides also with the occurrence of pronounced stress fibers. Although F-actin bundle formation could be the direct consequence of perinuclear actin release, we favor more elaborate models. F-actin formation is tightly controlled and a complicated cellular process [55]. Therefore, we speculate the uncoupling of nesprin-2 tethered stress fiber inducing or stabilizing factors (Fig. 10). Perinuclear actin defines nuclear shape and migration [47, 56]. Moreover, in *C. elegans*, kinesin-1 is required for nuclear migration [49]. Notably, nuclear migration rates are drastically reduced in nesprin-2 KASH-domain knockout brain cells [33]. Thus, nesprin-2 might directly account for the perinuclear cytoskeleton perturbations and the nuclear migration deficits exhibited by lamin A/C mutants [26, 57].

MT integrity is required for the organization of the Golgi apparatus, which plays key roles in directed secretion, cell polarity, and wound closure [2]. In addition, specific KLC1 isoforms associate with the Golgi complex [58]. Therefore, the Golgi deformities exhibited by nesprin-2 mutants may result from both KLC1 and MT-network defects.

Nesprin-2 controls centrosome attachment to the NE

Nesprin-2 KASH-domain knockout mouse data [33] as well as our DN-SUNL data indicate an essential function of

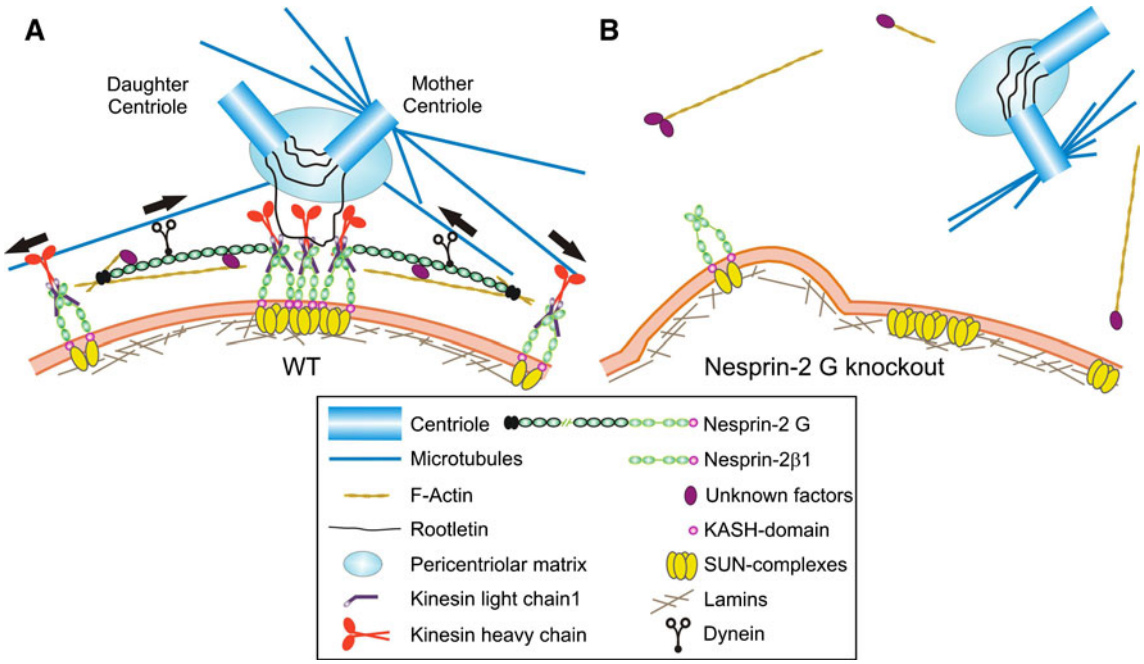

Fig. 10a, b Model of NE-mediated centrosomal and cytoskeletal anchorage. Comparison of nesprin-2/KLC1-dependent centrosomal positioning and cytoskeletal organization at the NE of WT (**a**) and nesprin-2 G–deficient cells (**b**). SUN-protein-tethered nesprin-2 KASH-isoform assemblies, kinesin-1 NE-associated complexes (MTs and rootletin), dynein, and unknown factors enable the physical linkage of the cytoskeleton and the centrosome to the NE. Dynein pulls the nucleus towards the centrosome, whereas active kinesin-1 pushes nuclei away. We hypothesize that when the nesprin-2 G scaffold is absent, the centrosome attachment site is severed and the cytoskeleton is detached, and that the MT-motor protein content at the NE is modulated

nesprin-2 in centrosome attachment to the NE. In contrast, a recent study [10] showed that nesprin-4 KASH-domain overexpression in HeLa cells did not perturb centrosome positioning, which might be explained by an incomplete displacement of all endogenous nesprin-2 isoforms. The compelling evidence that nesprin-2 G is involved in centrosomal tethering too implicates that both KASH- and actin-binding-domain-containing nesprin-2 isoforms have a role in centrosomal tethering. Taken together, our data combined with the results by Zhang et al. [33] suggest that, similar to lamin A/C [23, 59], nesprin-2 is also a positive regulator of centrosomal attachment.

MT- and NE-mediated mechanisms of centrosomal anchorage

The integrity of the MT network is essential for the physical anchorage of centrosomes at the NE [59, 60]. Interestingly, emerin, which is positioned in the outer nuclear membrane and which binds to nesprin-2, also facilitates centrosomal attachment by associating directly with MTs [59]. Hence, nesprin-2/kinesin-1 and nesprin-2/emerin complexes may physically link centrosomes to the NE surface via MTs. Several lines of evidence indicate, however, that centrosome-NE tethering is far more complex. For example, centrosomal tethering in *C. elegans* involves the minus-end-directed motor protein dynein [7]. Moreover, centrosomal tethering to the mammalian NE is currently conceived as the result of dynein-mediated pulling of the nuclei towards the centrosome, and centrosome detachment as the result of kinesin-1-mediated nuclear movement away from the centrosome [10, 33, 61].

In KLC1 knockout mice, the KHC behavior and localization are profoundly affected [62]. Furthermore, cargo binding and the presence of KLC subunits determine the activity of the kinesin complex [63, 64]. Hence, we envisage that the functions of nesprin/kinesin-1 complexes may differ in various cell types during the cell cycle and might be modulated spatially and temporally by further interactions. The latter is best exemplified in the kinesin-1 association with rootletin, which is a ubiquitous centrosomal component [65, 66]. Rootletin associates directly with the KLC N-termini [67]. Taking into account that the KLC1 C-terminus binds to nesprin-2 (this study), tripartite complexes with rootletin (putative centrosome attachment site) can be assumed. Interestingly, rootletin overexpression recruits both KLC and KHC, however, these resulting complexes neither recruit nor bind MTs [67].

The presence of centrosome attachment sites is reflected by microdomains built by SUN proteins at the inner nuclear membrane. Indeed, Sun1- and Sun2-deficient mice exhibit centrosome detachment [33]. Since centrosome-NE

tethering resists harsh biochemical purification procedures [68, 69], it is obvious that MT-independent tethering mechanisms must exist. All together, this evidence lead us to speculate that the controlled balance of plus- and minus-end-directed motor proteins as well as direct associations between the NE and centrosomal proteins themselves (including MTs) may result in proper centrosome positioning (Fig. 10).

In conclusion, our data show that nesprin-2 is a versatile protein that controls cytoskeleton organization, organelle positioning, KLC1 subcellular localization, and polarization of epithelial cells. However, further efforts have to be undertaken to elucidate how these vital functions are coordinated and coupled with extracellular and/or intracellular cues to master cellular behavior and tissue organization.

Acknowledgments We thank Drs. S.T. Brady, R.D. Vale, W.T. Dauer, C.J. Hutchinson, and U. Euteneuer for providing reagents. We thank Dr. Martin Goldberg for critically reading the manuscript and Drs. R. Foisner, P.J. Hussey, R. Quinlan, and A. Smertenko for valuable discussions, as well as M. Munck and R. Blau-Wasser for technical advice. This work was supported by a grant from the Deutsche Forschungsgemeinschaft (KA 2778/1-1), the St. Moritz-Foundation, and the Wellcome Trust.

References

1. Li R, Gundersen GG (2008) Beyond polymer polarity: how the cytoskeleton builds a polarized cell. Nat Rev Mol Cell Biol 9:860–873
2. Yadav S, Puri S, Linstedt AD (2009) Primary role for Golgi positioning in directed secretion, cell polarity, and wound healing. Mol Biol Cell 20:1728–1736
3. Starr DA (2007) Communication between the cytoskeleton and the nuclear envelope to position the nucleus. Mol Biosyst 3:583–589
4. Starr DA (2009) A nuclear-envelope bridge positions nuclei and moves chromosomes. J Cell Sci 122:577–586
5. Schneider M, Noegel AA, Karakesisoglou I (2008) KASH-domain proteins and the cytoskeletal landscapes of the nuclear envelope. Biochem Soc Trans 36:1368–1372
6. Shimanuki M, Miki F, Ding DQ, Chikashige Y, Hiraoka Y, Horio T, Niwa O (1997) A novel fission yeast gene, kms1+, is required for the formation of meiotic prophase-specific nuclear architecture. Mol Gen Genet 254:238–249
7. Malone CJ, Misner L, Le Bot N, Tsai MC, Campbell JM, Ahringer J, White JG (2003) The *C. elegans* hook protein, ZYG-12, mediates the essential attachment between the centrosome and nucleus. Cell 115:825–836
8. Patterson K, Molofsky AB, Robinson C, Acosta S, Cater C, Fischer JA (2004) The functions of Klarsicht and nuclear lamin in developmentally regulated nuclear migrations of photoreceptor cells in the Drosophila eye. Mol Biol Cell 15:600–610
9. Wilhelmsen K, Litjens SH, Kuikman I, Tshimbalanga N, Janssen H, van den Bout I, Raymond K, Sonnenberg A (2005) Nesprin-3, a novel outer nuclear membrane protein, associates with the cytoskeletal linker protein plectin. J Cell Biol 171:799–810
10. Roux KJ, Crisp ML, Liu Q, Kim D, Kozlov S, Stewart CL, Burke B (2009) Nesprin 4 is an outer nuclear membrane protein that can induce kinesin-mediated cell polarization. Proc Natl Acad Sci USA 106:2194–2199
11. Zhang Q, Ragnauth C, Greener MJ, Shanahan CM, Roberts RG (2002) The nesprins are giant actin-binding proteins, orthologous to Drosophila melanogaster muscle protein MSP-300. Genomics 80:473–481
12. Zhen YY, Libotte T, Munck M, Noegel AA, Korenbaum E (2002) NUANCE, a giant protein connecting the nucleus and actin cytoskeleton. J Cell Sci 115:3207–3222
13. Padmakumar VC, Abraham S, Braune S, Noegel AA, Tunggal B, Karakesisoglou I, Korenbaum E (2004) Enaptin, a giant actin-binding protein, is an element of the nuclear membrane and the actin cytoskeleton. Exp Cell Res 295:330–339
14. Dawe HR, Adams M, Wheway G, Szymanska K, Logan CV, Noegel AA, Gull K, Johnson CA (2009) Nesprin-2 interacts with meckelin and mediates ciliogenesis via remodelling of the actin cytoskeleton. J Cell Sci 122:2716–2726
15. Padmakumar VC, Libotte T, Lu W, Zaim H, Abraham S, Noegel AA, Gotzmann J, Foisner R, Karakesisoglou I (2005) The inner nuclear membrane protein Sun1 mediates the anchorage of Nesprin-2 to the nuclear envelope. J Cell Sci 118:3419–3430
16. Crisp M, Liu Q, Roux K, Rattner JB, Shanahan C, Burke B, Stahl PD, Hodzic D (2006) Coupling of the nucleus and cytoplasm: role of the LINC complex. J Cell Biol 172:41–53
17. Lu W, Gotzmann J, Sironi L, Jaeger VM, Schneider M, Luke Y, Uhlen M, Szigyarto CA, Brachner A, Ellenberg J, Foisner R, Noegel AA, Karakesisoglou I (2008) Sun1 forms immobile macromolecular assemblies at the nuclear envelope. Biochim Biophys Acta 1783:2415–2426
18. Muchir A, van Engelen BG, Lammens M, Mislow JM, McNally E, Schwartz K, Bonne G (2003) Nuclear envelope alterations in fibroblasts from LGMD1B patients carrying nonsense Y259X heterozygous or homozygous mutation in lamin A/C gene. Exp Cell Res 291:352–362
19. Libotte T, Zaim H, Abraham S, Padmakumar VC, Schneider M, Lu W, Munck M, Hutchison C, Wehnert M, Fahrenkrog B, Sauder U, Aebi U, Noegel AA, Karakesisoglou I (2005) Lamin A/C dependent localization of Nesprin-2, a giant scaffolder at the nuclear envelope. Mol Biol Cell 16:3411–3424
20. Kandert S, Lüke Y, Kleinhenz T, Neumann S, Lu W, Jaeger VM, Munck M, Wehnert M, Müller CR, Zhou Z, Noegel AA, Dabauvalle MC, Karakesisoglou I (2007) Nesprin-2 giant safeguards nuclear envelope architecture in LMNA S143F progeria cells. Hum Mol Genet 16:2944–2959
21. Broers JL, Ramaekers FC, Bonne G, Yaou RB, Hutchison CJ (2006) Nuclear lamins: laminopathies and their role in premature ageing. Physiol Rev 86:967–1008
22. Mattout A, Dechat T, Adam SA, Goldman RD, Gruenbaum Y (2006) Nuclear lamins, diseases and aging. Curr Opin Cell Biol 18:335–341
23. Lee JS, Hale CM, Panorchan P, Khatau SB, George JP, Tseng Y, Stewart CL, Hodzic D, Wirtz D (2007) Nuclear lamin A/C deficiency induces defects in cell mechanics, polarization, and migration. Biophys J 93:2542–2552
24. Hale CM, Shrestha AL, Khatau SB, Stewart-Hutchinson PJ, Hernandez L, Stewart CL, Hodzic D, Wirtz D (2008) Dysfunctional connections between the nucleus and the actin and microtubule networks in laminopathic models. Biophys J 95:5462–5475
25. Stewart-Hutchinson PJ, Hale CM, Wirtz D, Hodzic D (2008) Structural requirements for the assembly of LINC complexes and their function in cellular mechanical stiffness. Exp Cell Res 314:1892–1905

26. Houben F, Willems CH, Declercq IL, Hochstenbach K, Kamps MA, Snoeckx LH, Ramaekers FC, Broers JL (2009) Disturbed nuclear orientation and cellular migration in A-type lamin deficient cells. Biochim Biophys Acta 1793:312–324
27. Gros-Louis F, Dupre N, Dion P, Fox MA, Laurent S, Verreault S, Sanes JR, Bouchard JP, Rouleau GA (2007) Mutations in SYNE1 lead to a newly discovered form of autosomal recessive cerebellar ataxia. Nat Genet 39:80–85
28. Zhang Q, Bethmann C, Worth NF, Davies JD, Wasner C, Feuer A, Ragnauth CD, Yi Q, Mellad JA, Warren DT, Wheeler MA, Ellis JA, Skepper JN, Vorgerd M, Schlotter-Weigel B, Weissberg PL, Roberts RG, Wehnert M, Shanahan CM (2007) Nesprin-1 and -2 are involved in the pathogenesis of Emery Dreifuss muscular dystrophy and are critical for nuclear envelope integrity. Hum Mol Genet 16:2816–2833
29. Attali R, Warwar N, Israel A, Gurt I, McNally E, Puckelwartz M, Glick B, Nevo Y, Ben-Neriah Z, Melki J (2009) Mutation of SYNE-1, encoding an essential component of the nuclear lamina, is responsible for autosomal recessive arthrogryposis. Hum Mol Genet 18:3462–3469
30. Puckelwartz MJ, Kessler E, Zhang Y, Hodzic D, Randles KN, Morris G, Earley JU, Hadhazy M, Holaska JM, Mewborn SK, Pytel P, McNally EM (2009) Disruption of nesprin-1 produces an Emery Dreifuss muscular dystrophy-like phenotype in mice. Hum Mol Genet 18:607–620
31. Luke Y, Zaim H, Karakesisoglou I, Jaeger VM, Sellin L, Lu W, Schneider M, Neumann S, Beijer A, Munck M, Padmakumar VC, Gloy J, Walz G, Noegel AA (2008) Nesprin-2 Giant (NUANCE) maintains nuclear envelope architecture and composition in skin. J Cell Sci 121:1887–1898
32. Zhang X, Xu R, Zhu B, Yang X, Ding X, Duan S, Xu T, Zhuang Y, Han M (2007) Syne-1 and Syne-2 play crucial roles in myonuclear anchorage and motor neuron innervation. Development 134:901–908
33. Zhang X, Lei K, Yuan X, Wu X, Zhuang Y, Xu T, Xu R, Han M (2009) SUN1/2 and Syne/Nesprin-1/2 complexes connect centrosome to the nucleus during neurogenesis and neuronal migration in mice. Neuron 64:173–187
34. Vale RD, Reese TS, Sheetz MP (1985) Identification of a novel force-generating protein, kinesin, involved in microtubule-based motility. Cell 42:39–50
35. Vale RD (2003) The molecular motor toolbox for intracellular transport. Cell 112:467–480
36. Paddison PJ, Caudy AA, Bernstein E, Hannon GJ, Conklin DS (2002) Short hairpin RNAs (shRNAs) induce sequence-specific silencing in mammalian cells. Genes Dev 16:948–958
37. Elbashir SM, Harborth J, Lendeckel W, Yalcin A, Weber K, Tuschl T (2001) Duplexes of 21-nucleotide RNAs mediate RNA interference in cultured mammalian cells. Nature 411:494–498
38. Evan GI, Lewis GK, Ramsay G, Bishop JM (1985) Isolation of monoclonal antibodies specific for human c-myc proto-oncogene product. Mol Cell Biol 5:3610–3616
39. Xiong H, Rivero F, Euteneuer U, Mondal S, Mana-Capelli S, Larochelle D, Vogel A, Gassen B, Noegel AA (2008) Dictyostelium Sun-1 connects the centrosome to chromatin and ensures genome stability. Traffic 9:708–724
40. Noegel AA, Blau-Wasser R, Sultana H, Muller R, Israel L, Schleicher M, Patel H, Weijer CJ (2004) The cyclase-associated protein CAP as regulator of cell polarity and cAMP signaling in Dictyostelium. Mol Biol Cell 15:934–945
41. Laemmli UK (1970) Cleavage of structural proteins during the assembly of the head of bacteriophage T4. Nature 227:680–685
42. Towbin H, Staehelin T, Gordon J (1979) Electrophoretic transfer of proteins from polyacrylamide gels to nitrocellulose sheets: procedure and some applications. Proc Natl Acad Sci USA 76:4350–4354
43. Konecna A, Frischknecht R, Kinter J, Ludwig A, Steuble M, Meskenaite V, Indermuhle M, Engel M, Cen C, Mateos JM, Streit P, Sonderegger P (2006) Calsyntenin-1 docks vesicular cargo to kinesin-1. Mol Biol Cell 17:3651–3663
44. Blum H, Beier H, Gross HJ (1987) Improved silver staining of plant-proteins, RNA and DNA in polyacrylamide gels. Electrophoresis 8:93–99
45. Wang Q, Du X, Cai Z, Greene MI (2006) Characterization of the structures involved in localization of the SUN proteins to the nuclear envelope and the centrosome. DNA Cell Biol 25:554–562
46. Kodama A, Karakesisoglou I, Wong E, Vaezi A, Fuchs E (2003) ACF7: an essential integrator of microtubule dynamics. Cell 115:343–354
47. Gomes ER, Jani S, Gundersen GG (2005) Nuclear movement regulated by Cdc42, MRCK, myosin, and actin flow establishes MTOC polarization in migrating cells. Cell 121:451–463
48. Gotzmann J, Foisner R (2006) A-type lamin complexes and regenerative potential: a step towards understanding laminopathic diseases? Histochem Cell Biol 125:33–41
49. Meyerzon M, Fridolfsson HN, Ly N, McNally FJ, Starr DA (2009) UNC-83 is a nuclear-specific cargo adaptor for kinesin-1-mediated nuclear migration. Development 136:2725–2733
50. Stenoien DL, Brady ST (1997) Immunochemical analysis of kinesin light chain function. Mol Biol Cell 8:675–689
51. Verhey KJ, Lizotte DL, Abramson T, Barenboim L, Schnapp BJ, Rapoport TA (1998) Light chain-dependent regulation of Kinesin's interaction with microtubules. J Cell Biol 143:1053–1066
52. Glater EE, Megeath LJ, Stowers RS, Schwarz TL (2006) Axonal transport of mitochondria requires milton to recruit kinesin heavy chain and is light chain independent. J Cell Biol 173:545–557
53. Koizumi H, Gleeson JG (2009) Sun proteins enlighten nuclear movement in development. Neuron 64:147–149
54. Higginbotham HR, Gleeson JG (2007) The centrosome in neuronal development. Trends Neurosci 30:276–283
55. Pollard TD, Cooper JA (2009) Actin, a central player in cell shape and movement. Science 326:1208–1212
56. Khatau SB, Hale CM, Stewart-Hutchinson PJ, Patel MS, Stewart CL, Searson PC, Hodzic D, Wirtz D (2009) A perinuclear actin cap regulates nuclear shape. Proc Natl Acad Sci USA 106:19017–19022
57. Mejat A, Decostre V, Li J, Renou L, Kesari A, Hantai D, Stewart CL, Xiao X, Hoffman E, Bonne G, Misteli T (2009) Lamin A/C-mediated neuromuscular junction defects in Emery-Dreifuss muscular dystrophy. J Cell Biol 184:31–44
58. Gyoeva FK, Bybikova EM, Minin AA (2000) An isoform of kinesin light chain specific for the Golgi complex. J Cell Sci 113:2047–2054
59. Salpingidou G, Smertenko A, Hausmanowa-Petrucewicz I, Hussey PJ, Hutchison CJ (2007) A novel role for the nuclear membrane protein emerin in association of the centrosome to the outer nuclear membrane. J Cell Biol 178:897–904
60. Meraldi P, Nigg EA (2001) Centrosome cohesion is regulated by a balance of kinase and phosphatase activities. J Cell Sci 114:3749–3757
61. Splinter D, Tanenbaum ME, Lindqvist A, Jaarsma D, Flotho A, Yu KL, Grigoriev I, Engelsma D, Haasdijk ED, Keijzer N, Demmers J, Fornerod M, Melchior F, Hoogenraad CC, Medema RH, Akhmanova A (2010) Bicaudal D2, dynein, and kinesin-1 associate with nuclear pore complexes and regulate centrosome and nuclear positioning during mitotic entry. PLoS Biol 8:e1000350
62. Rahman A, Kamal A, Roberts EA, Goldstein LS (1999) Defective kinesin heavy chain behavior in mouse kinesin light chain mutants. J Cell Biol 146:1277–1288
63. Cai D, Hoppe AD, Swanson JA, Verhey KJ (2007) Kinesin-1 structural organization and conformational changes revealed by FRET stoichiometry in live cells. J Cell Biol 176:51–63

64. Blasius TL, Cai D, Jih GT, Toret CP, Verhey KJ (2007) Two binding partners cooperate to activate the molecular motor Kinesin-1. J Cell Biol 176:11–17
65. Bahe S, Stierhof YD, Wilkinson CJ, Leiss F, Nigg EA (2005) Rootletin forms centriole-associated filaments and functions in centrosome cohesion. J Cell Biol 171:27–33
66. Yang J, Adamian M, Li T (2006) Rootletin interacts with C-Nap1 and may function as a physical linker between the pair of centrioles/basal bodies in cells. Mol Biol Cell 17:1033–1040
67. Yang J, Li T (2005) The ciliary rootlet interacts with kinesin light chains and may provide a scaffold for kinesin-1 vesicular cargos. Exp Cell Res 309:379–389
68. Bornens M (1977) Is the centriole bound to the nuclear membrane? Nature 270:80–82
69. Nadezhdina ES, Fais D, Chentsov YS (1979) On the association of centrioles with the interphase nucleus. Eur J Cell Biol 19:109–115